Vibrational Energy Flow Controls Internal Conversion in a Transition Metal Complex

*Gordon J. Hedley, Arvydas Ruseckas, and Ifor D. W. Samuel**

Supporting Information

1. Experimental Methods

1.1. Upconversion Setup

Ultrafast luminescence dynamics were recorded using upconversion spectroscopy. Briefly, the tunable 750-850 nm, 100 fs (FWHM), 80 MHz output of a Ti:Sapphire oscillator was directed into the upconversion setup (FOG100, CDP Systems). The second harmonic of the laser was generated in a type 1 Beta Barium Borate (BBO) crystal (1 mm thickness), producing an excitation beam (nominally λ = 400 nm, ~ 60 mW) and a gating beam (nominally λ = 800 nm, ~ 40 mW). The two beams were passed through a beam-splitter and the gating beam was sent down an optical delay line. The excitation beam was focused onto the sample space and a second lens was used to collect and collimate luminescence from the sample. The sample space itself is comprised of a rotating cuvette, which consists of two quartz windows sandwiching a spacer ring that holds the sample solution (optical path length 0.5 mm). The cell is rotated to avoid sample photodegradation due to the focused excitation beam that is incident upon it. The solution was found to be photostable for ~ 100 hours of laser exposure and was changed before this time was reached to ensure results were not compromised – the absorption

spectrum of the sample was regularly checked for any signs of degradation. The sample luminescence and the gating pulse were brought together on a type 1 BBO crystal (0.5 mm thickness) by an achromatic lens and the sum-frequency of the two was generated. The upconverted light in the UV was collimated by a second achromatic lens before being spatially filtered with an aperture and spectrally filtered with a dielectric filter with high reflectance at 400 nm to remove any residual excitation and a schott glass filter (UV pass). The resultant light is fed into a monochromator (CDP Systems model 2022) before being detected with a photomultiplier tube. Temporal dynamics are recorded by moving the delay line on the gating arm – this occurs by computer control with the "Lumex" software provided by CDP Systems that controls both the delay line motion and the photomultiplier tube counting. Setting and optimization of the upconversion setup at each detection wavelength was achieved with a sample cell filled with an appropriate laser dye solution. This highly emissive material gave a strong signal to enable optimization of upconversion crystal angle and spatial overlap of the gate and luminescence spots on the crystal. The instrument response function (IRF) of the system was obtained by upconverting the Raman signal of deionised water, and was found to be 285 fs (FWHM) with 400 nm excitation and 310 fs (FWHM) with 380 nm excitation.

1.2. Transient Absorption Setup

Transient absorption dynamics were recorded using the output of a regeneratively amplified Ti:Sapphire system. The pump of 400 nm was synchronously chopped at 2.5 kHz and sent along a delay line, while the probe, generated by a TOPAS-White system (500-1000 nm, ~30-50 fs FWHM) was operated at 5 kHz. Both pump and probe were spatially overlapped on the sample, with the rotating cuvette from the upconversion setup being used (optical path length 0.5 mm). Schott glass filters and pin-holes were used to spectrally and spatially filter out the 400 nm pump after the sample before the probe was detected with a silicon photodiode. Lock-in amplifiers were used to improve the signal/noise, with the probe signal at 5 kHz acting as a reference. Temporal dynamics were recorded by moving the delay line and thus changing the time between the arrival of the pump and probe pulses. Control of the delay line and recording of the photodiode signal was achieved with a homebuilt labview program.

1.3. Sample Preparation

The iridium complex used in these studies was bis(2-(9,9-dibutylfluorenyl)-1-isoquinoline(acetylacetonate) iridium (III), denoted as $Ir(dbfliq)_2acac$, it was purchased from American Dye Source Inc. and was used without further purification. The material was dissolved in tetrahydrofuran (THF) (spectroscopic grade, Sigma Aldrich Co.) at a concentration of 2 mg in 1 ml.

2. Spectral Fitting & Transition Dipole Moment Calculations

Absorption and photoluminescence spectra were converted to an energy scale (eV) and fitted with Gaussian functions. Fitting parameters are shown in Table S1. The residuals of the absorption spectrum fits (experimental data - fit) are shown in Figure S1, with residual values of 1% of the total signal level being found in the $S_{1\text{-}3}$ region.

Table S1: Fitting parameters of absorption and PL spectra to the superposition of Gaussian functions, indicating the central energy of Gaussian and full-width half maximum.

Transition	Central Energy (eV)	FWHM (eV)
$S_0 \rightarrow L_2$ (Abs.)	3.86	0.5
$S_0 \rightarrow L_1$ (Abs.)	3.32	0.52
$S_0 \rightarrow S_3$ (Abs.)	2.77	0.25
$S_0 \rightarrow S_2$ (Abs.)	2.47	0.25
$S_0 \rightarrow S_1$ (Abs.)	2.21	0.25
$S_0 \rightarrow T_1$ (Abs.)	1.95	0.12
$T_1 \rightarrow S_0$ (0-0) PL	1.88	0.14
$T_1 \rightarrow S_0$ (0-1) PL	1.74	0.15
$T_1 \rightarrow S_0$ (0-2) PL	1.6	0.15

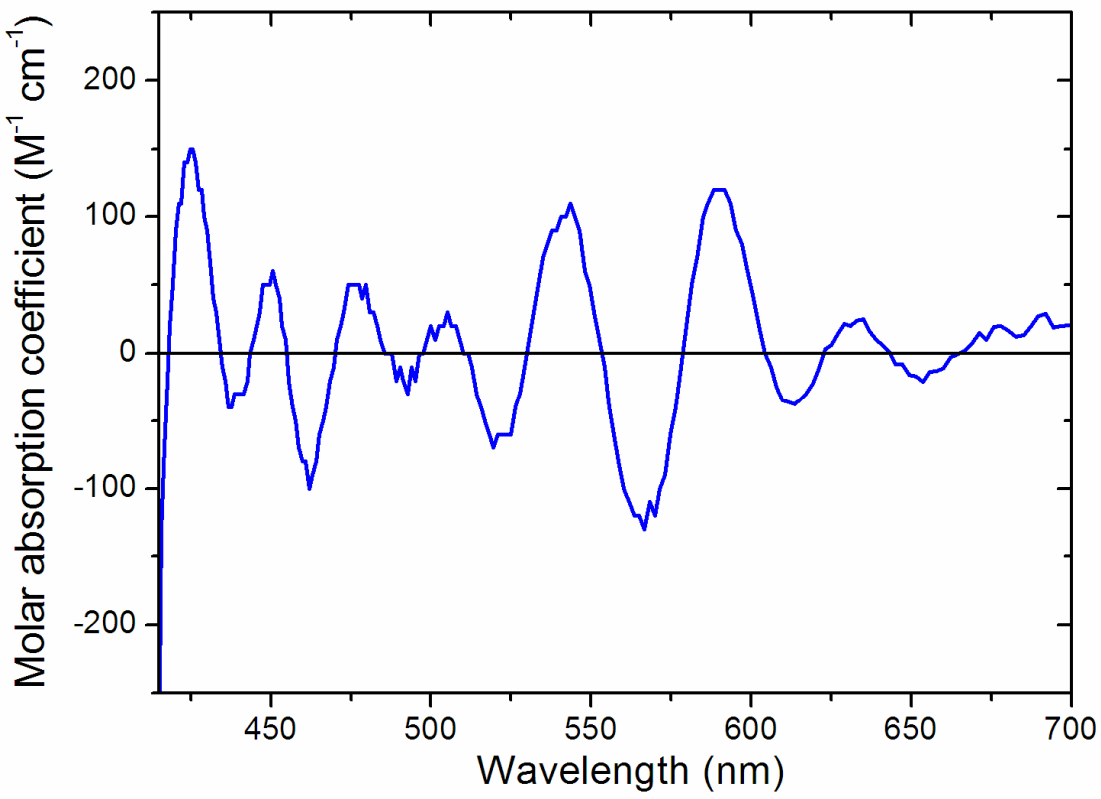

Figure S1: Residual signal level after the experimental absorption spectrum is subtracted from the superposition of Gaussian functions. Residual values are ~ 1% of the total signal level in the $S_{1\text{-}3}$ region (400-600 nm).

Transition dipole moment calculations were undertaken to help identify and support the assignments made to the features of the absorption spectrum. To test the validity of the calculated values it is first worth testing this approach by looking at the emitting ^{3}MLCT state. The oscillator strength, f, is defined by equation S1:[1]

$$f = \frac{4\pi m_e \upsilon}{3e^2\hbar}|\mu|^2 \qquad \text{(S1)}$$

where m_e is the mass of the electron, υ is the intensity weighted averaged emission frequency in hertz, e is the charge of an electron, $\hbar$ is planck's constant divided by 2π and μ is the transition dipole moment. For luminescence the dipole moment is defined by equation S2:[2, 3]

$$\mu^2 = \frac{3\pi\varepsilon_0\hbar^4 c^3 \left\langle E^{-3} \right\rangle}{n_0 \tau_R} \qquad \text{(S2)}$$

where ε_0 is the vacuum dielectric constant, $\hbar$ is planck's constant divided by 2π, c is the speed of light, n_0 is the refractive index of the solvent, τ_R is the radiative lifetime and $\left\langle E^{-3} \right\rangle$ is the intensity weighted average of the luminescence spectrum, defined by equation S3:

$$\left\langle E^{-3} \right\rangle = \frac{\int E^{-3} I(E) dE}{\int I(E) dE} \qquad \text{(S3)}$$

where E is the energy of the luminescence of intensity I in joules. The photoluminescence quantum yield (PLQY) of $Ir(dbfliq)_2acac$ was measured by dissolving the material in THF at a concentration that gave an absorbance of 0.1, degassing with three freeze-pump-thaw cycles and measuring the PL spectrum, with a quinine sulphate solution used as a reference. The PLQY value was determined to be 21%. The degassed luminescence lifetime was recorded by using a time correlated single photon counting setup and was found to be 1 μs. Consequently by use of equation S4 the radiative lifetime can be deduced, and was found to be 4 μs.

$$\tau_R = \frac{\tau_{PL}}{PLQY} \qquad \text{(S4)}$$

Hence for $Ir(dbfliq)_2acac$, taking the recorded PL spectrum, the refractive index of THF of 1.4 and using the calculated radiative rate of 4 μs, a dipole moment of 0.41 D for the emitting ^{3}MLCT state is calculated, which gives an oscillator strength of 1.1×10^{-3}. Comparing this value with the number that can be calculated for the absorption spectrum feature T_1 identified using equation S5:[2]

$$\mu^2 = 9.186 \times 10^{-3} n_0 \int \left[\frac{\varepsilon(\upsilon)}{\upsilon} \right] d\upsilon \qquad \text{(S5)}$$

where n_0 is the refractive index of the solvent and the integral is the intensity weighted average of the identified absorption feature area. The calculated value of the T_1 Gaussian is thus 0.54 D, which gives an oscillator strength of 2.2×10^{-3}, a number in good

agreement with the value calculated from the PL spectrum. These numbers are congruent with those reported for time dependent density functional theory (TDDFT) calculations by Nozaki on the prototypical $Ir(ppy)_3$ complex,[4] where an oscillator strength of ~ $8.5x10^{-4}$ is calculated for the highest triplet sublevel.

It is therefore valid to use the absorption spectrum as a source for obtaining transition dipole moment and oscillator strength values. Doing this for the identified features of the spectrum produces values as shown in Table S2.

Table S2: Experimental transition dipole moments and oscillator strengths obtained using equations S1-3 of optical transitions identified in absorption and PL spectra.

Transition	Transition Dipole Moment (Debye)	Oscillator Strength	Assignment
$T_1 \rightarrow S_0$ (PL)	0.41	0.001	^{3}MLCT
$S_0 \rightarrow T_1$ (Abs.)	0.54	0.002	^{3}MLCT
$S_0 \rightarrow S_1$ (Abs.)	2.25	0.042	^{1}MLCT
$S_0 \rightarrow S_2$ (Abs.)	2.52	0.059	^{1}MLCT
$S_0 \rightarrow S_3$ (Abs.)	2.53	0.067	^{1}MLCT
$S_0 \rightarrow L_1$ (Abs.)	8.04	0.815	Ligand Centered

3. Ultrafast Luminescence fitting – Global Analysis

3.1. Methodology & Results

Ultrafast luminescence kinetics across the region 460-580 nm were globally analyzed using the "Globals WE" software package developed at the Laboratory for Fluorescence Dynamics at the University of Illinois at Urbana-Champaign.[5] The dataset at each wavelength was acquired by averaging numerous scans, with standard error in the mean values calculated at each point in each dataset from the individual scans. The fitting software package took all 12 datasets and fitted globally to find the global reduced chi-square minimum, the errors at each point in each dataset being used to calculate the individual wavelength and global reduced chi-square values. Fitting was performed presuming a consecutive relaxation scheme where the decay-time of S_3 was used as the rise-time of S_2 and the decay of S_2 was used as the rise-time of S_1. The fitting software allowed for the use of custom fitting equations, and our relaxation scheme was implemented using an equation as derived from solving a three state consecutive rate equation (main text, equation 1).

Seeded with sensible values the global fitting software iterated to find the reduced-chi squared minimum. The best-fit results are shown below, with parameters detailed in Table S3 and data and fits for all 14 wavelengths shown in Figure S2.

Table S3: Global Analysis best-fit parameters, overall and for each of the 12 wavelengths included in the global fit. Global amplitudes represent the multiplier on the individual amplitude components at each wavelength – all data as globally analyzed was wavelength intensity sensitivity corrected for the instrument as discussed in the manuscript.

		τ_1 (fs)	**τ_2 (fs)**	**τ_3 (fs)**	**Global Rχ^2**
Global Variables →		10	65	75	1.37976
Emission wavelength (nm)	**Global Amplitude**	**A_1**	**A_2**	**A_3**	**Local Rχ^2**
460	0.563	1	0	0	2.13177
480	0.88	0.462	0.538	0	1.88416
490	1	0.085	0.915	0	0.97182
500	0.687	0	1	0	1.71178
510	0.599	0	0.929	0.071	2.42487
520	0.469	0	0.727	0.273	1.98215
530	0.3	0	0.428	0.572	0.88047
540	0.345	0	0.318	0.682	1.29268
550	0.248	0	0	1	1.18026
560	0.227	0	0	1	1.02147
570	0.169	0	0	1	0.78864
580	0.168	0	0	1	1.01976

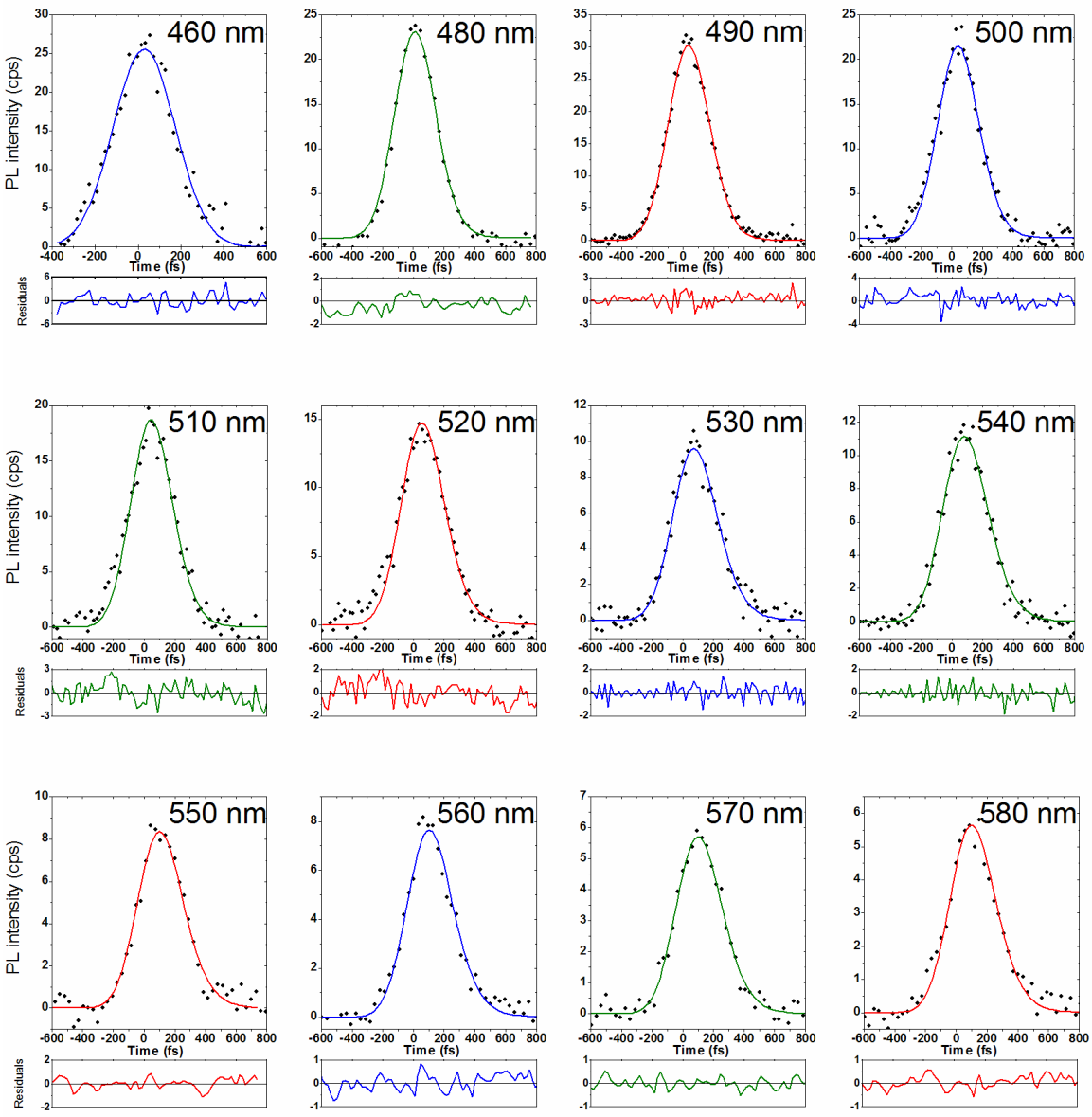

Figure S2: Ultrafast luminescence data (closed circles), global fits (solid lines) and residuals (beneath each window) for all 12 wavelengths that were globally analyzed.

3.2. Error Estimates

3.2.1. Tau 1

Direct fitting of τ_1 can only tell us that it is instrument limited (less than 50 fs) and so the time constant of S_3 decay has been deduced by finding the sensitivity of τ_1 to the decay associated fluorescence spectrum (DAFS) amplitude. Requiring the S_3 emission to lie on or close to the S_3 absorption Gaussian indicates that $\tau_1 < 20$ fs, with a value of 10 fs used in the global analysis. The variation of the S_3 amplitude with variation of τ_1 is shown in Figure S3 below, showing the amplitudes produced for τ_1 values of 10, 20, 30 and 50 fs.

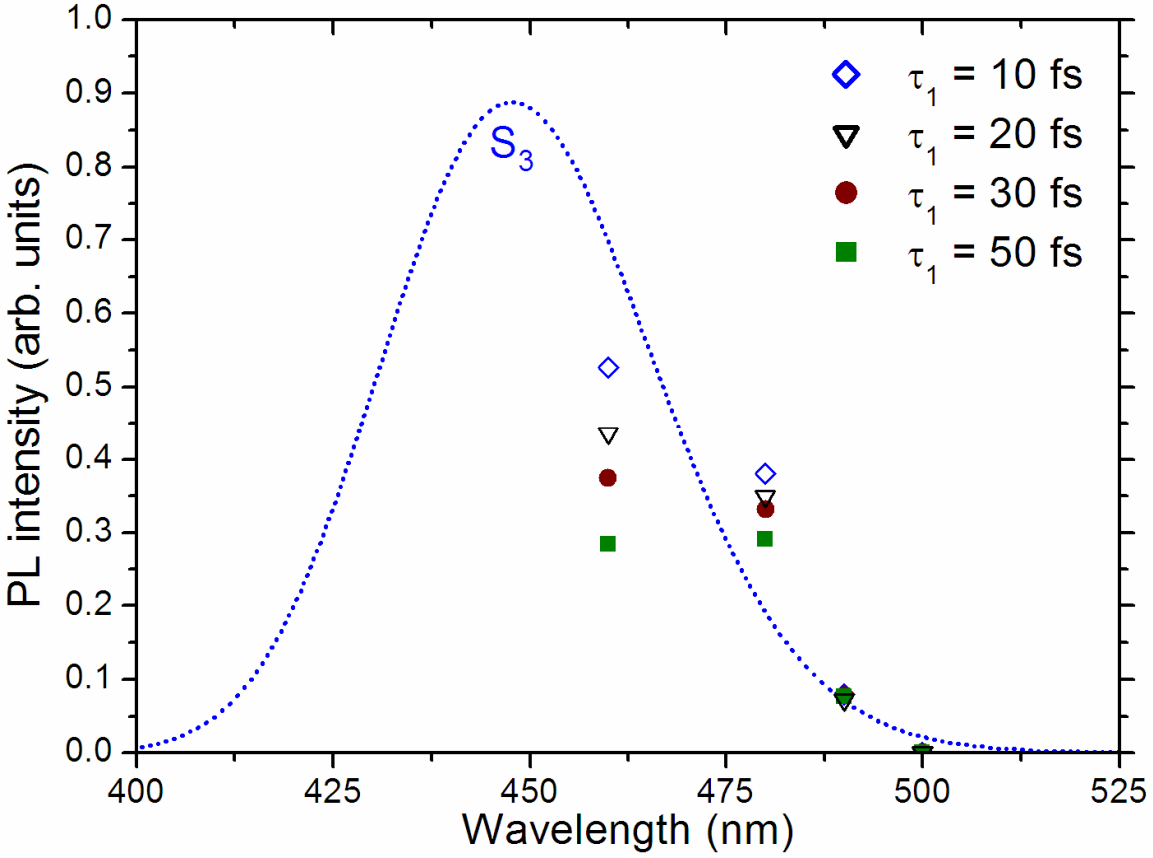

Figure S3: DAFS for variation of τ_1. Open diamonds indicate a time constant of 10 fs, open triangles 20 fs, closed circles 30 fs and closed squares 50 fs. τ_1 is thus said to be < 20 fs based on the required time constants to produce amplitudes that follow the S_3 absorption Gaussian.

3.2.2. Tau 2 & 3

Judging parameter uncertainty is an important part of an overall experimental analysis. Support plane analysis – the exploration of the reduced chi-squared (χ^2_R) surface – is regarded as one of the better ways of determining reasonable uncertainties of fitted parameters. Global analysis can help to generate a lower degree of uncertainty when a support plane analysis is undertaken, as the large number of combined datasets helps to reduce the uncertainty threshold.

Our support plane analysis was undertaken using calculated confidence intervals, as described by Lakowicz.[6] Briefly, the confidence interval is described as the χ^2_R value at which the probability, P, is equal to 0.32, i.e. the value of the χ^2_R is one standard deviation away from the χ^2_R minimum. This value is defined by equation S7 below:[6]

$$F_{\chi} = \frac{\chi^2_R(par)}{\chi^2_R(\min)} = 1 + \frac{p}{\upsilon} F(p,\nu,P) \qquad \text{(S7)}$$

where F_χ is the multiplier on the χ^2_R minimum to give the value of χ^2_R at one standard deviation of error (χ^2_R (par)), p is the number of fitting parameters, υ is the degrees of freedom and F(p,υ,P) is the F-Statistic value with p parameters, υ degrees of freedom and a probability, P, of 0.32. Inputting the values found from the data used in the global analysis, p = 6 and υ = 924 gives an F-Statistic value of 1.16, which implies that F_χ = 1.0075. Thus given that the global χ^2_R was found to be 1.37976, the one standard deviation value of χ^2_R is 1.39. Uncertainty in parameters can thus be estimated by

refitting the global data while fixing the value of a parameter (leaving all others free), recording the χ^2_R value and finding when this becomes larger than the one standard deviation value calculated above. Visualization of the results of this procedure normally takes the form of a two dimensional plot of χ^2_R vs. parameter value, producing a parabola with a horizontal line indicating the error threshold. In this work, however we have variation of a number of parameters, and thus a three dimensional contour plot is produced, comprising of a 7x9 matrix of χ^2_R values, as shown below in Figure S4 when varying τ_2 and τ_3. A ring can be traced (thick black line) at the one standard deviation contour line, and this defines the errors for the two time constants, stated as ± 7 for τ_2 and ± 12 fs for τ_3.

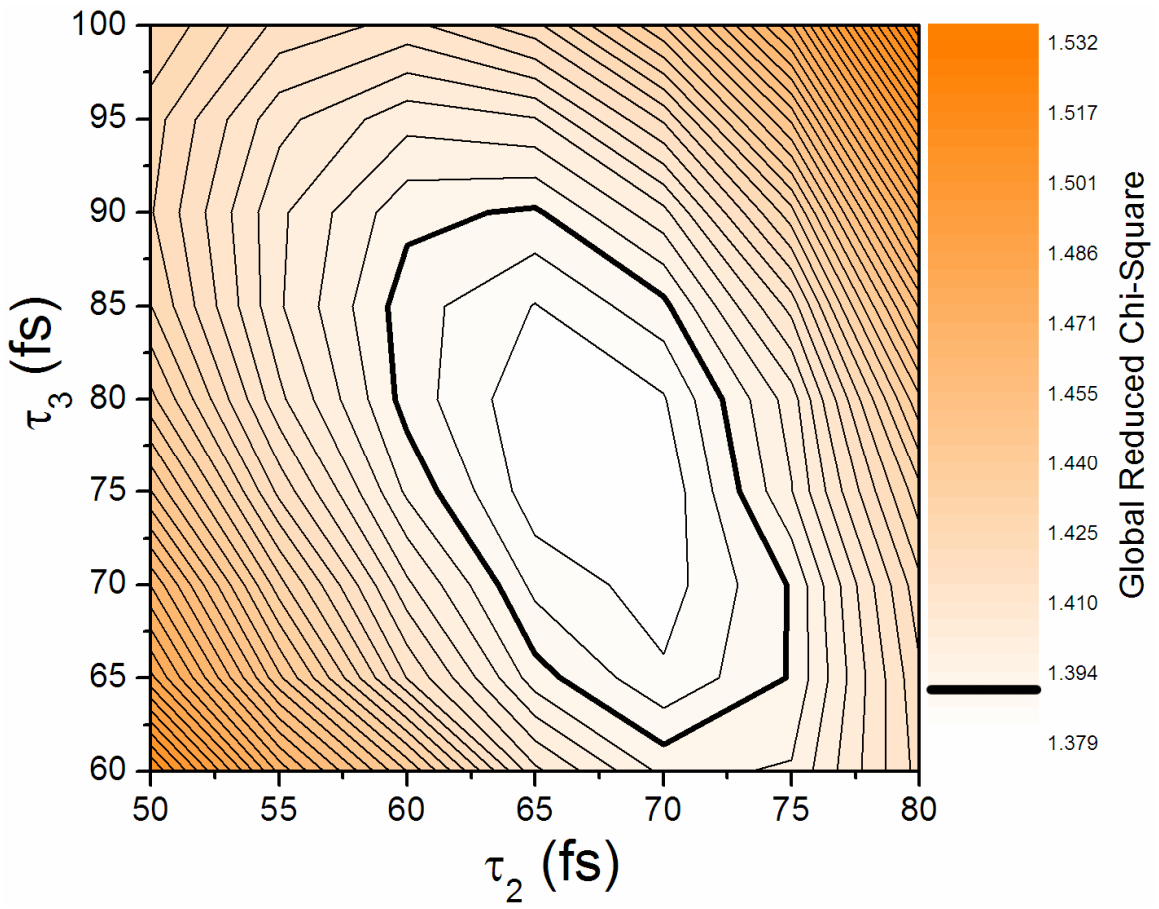

Figure S4: Contour plot of global reduced chi-square surface at τ_1 = 10 fs when varying τ_2 and τ_3 with all other parameters left free. The global minimum of the surface is found to be at τ_2 = 65 fs and τ_3 = 75 fs. Quoted errors of ± 7 and ± 12 fs are derived from the increase in the reduced chi-square value of 1 standard deviation, as defined by F-Statistics, and is indicated with the thick black line.

4. Singular Value Decomposition

Singular value decomposition (SVD) can act as a useful mathematical technique to help better elucidate the underlying spectro-temporal dynamics. This is achieved by separating the spectral and temporal components into two separate matrices, and has been extensively discussed in detail elsewhere.[7, 8] Briefly, the 12 recorded wavelengths can be assembled as an M x N matrix, with M wavelengths and N data points per wavelength. SVD decomposes the M x N matrix into two orthogonal matrices of M x M and N x N and an S matrix whose diagonal elements represent the singular values which can be utilized to determine the number of components of significance that are in the global dataset. Figure S5, showing the singular value matrix elements with increasing index values, indicating at least three components of significance exist within the global dataset.

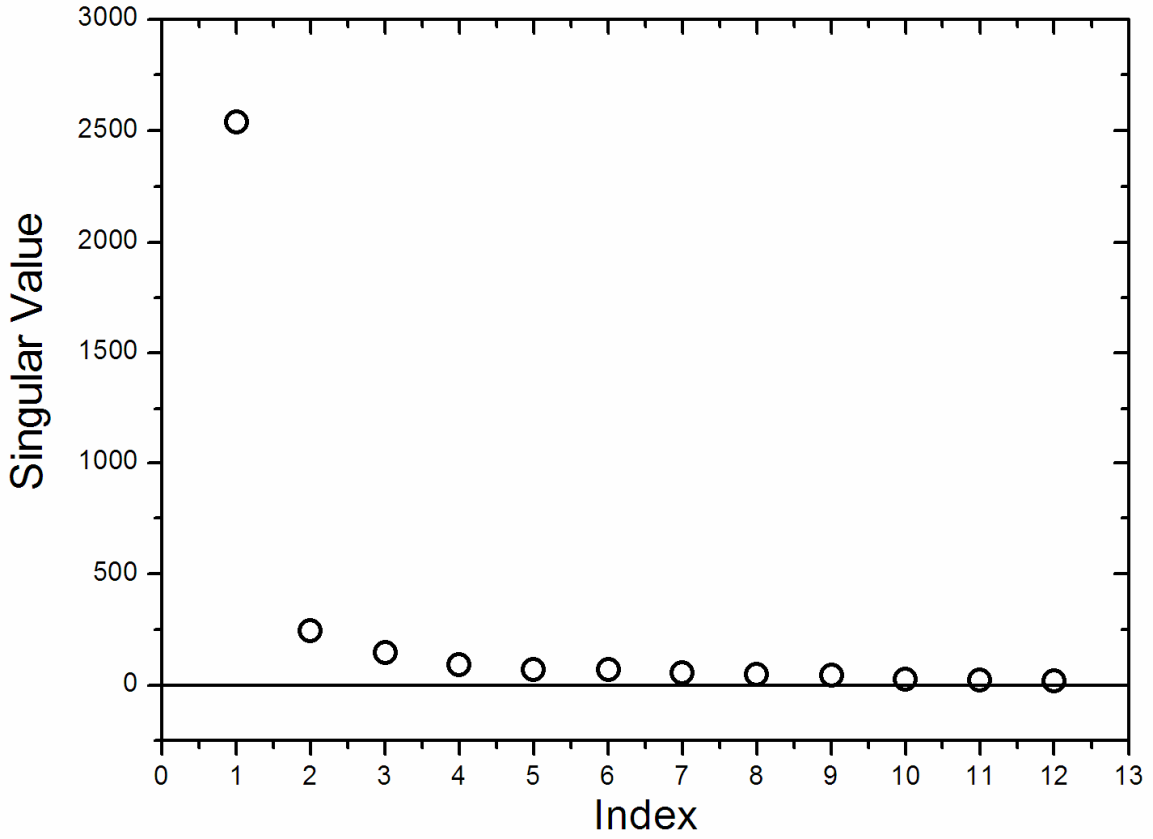

Figure S5: SVD plot showing, the singular matrix plotted against index number. A y=0 line is also shown to show the significance of the first three components.

5. Variation of Excitation Energy

Variation of excitation energy was utilized to test the dependence of stored energy inside the molecule against the rates of IC and ISC. Shown below in Figure S6 are the kinetics recorded at a detection wavelength of 550 nm, with 400 nm excitation (closed circles) and 425 nm (open circles). The solid line represents a fit with a rise-time of 65 fs and a decay of 75 fs. It can be seen that both excitation wavelengths produce kinetics that are the same.

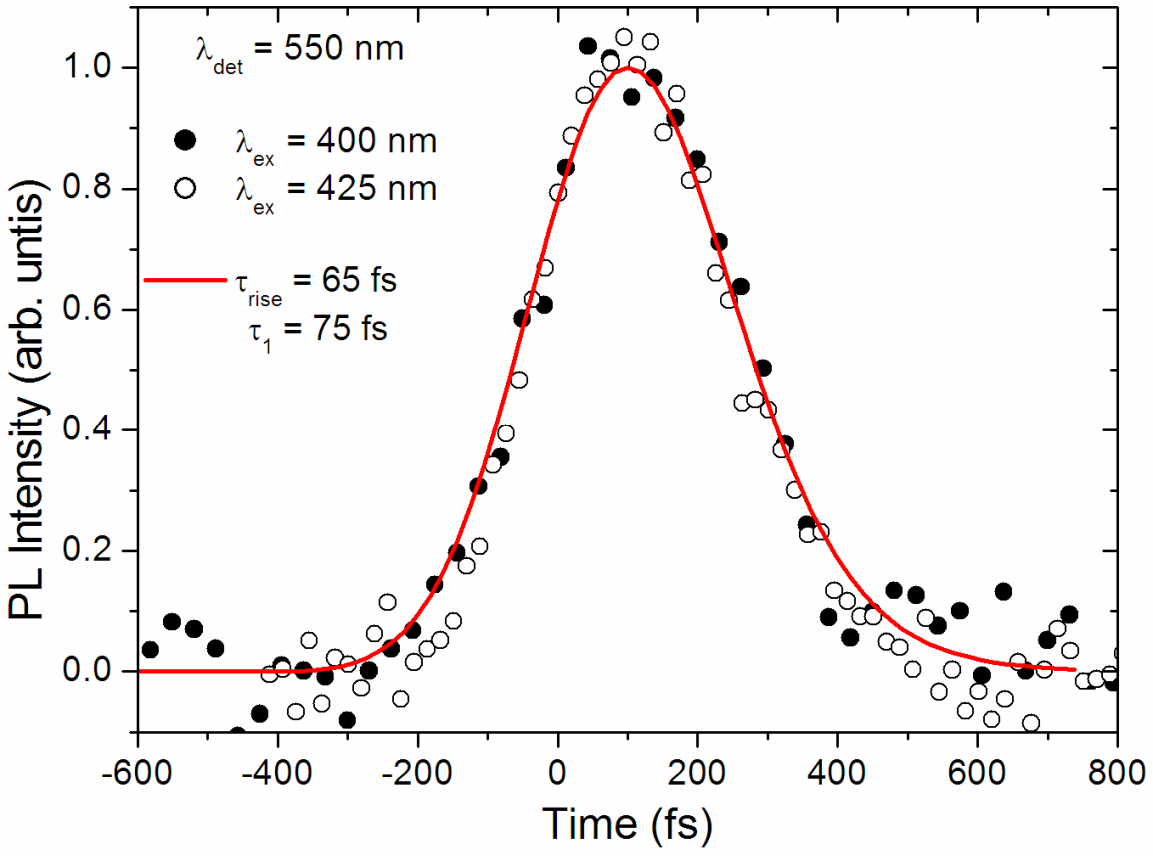

Figure S6: Ultrafast luminescence kinetics at 550 nm with variation of excitation wavelength, 400 nm (closed circles) and 425 nm (open circles).

6. Ultrafast Luminescence at Lower Detection Energy

Ultrafast luminescence dynamics at longer detection wavelengths show slower kinetics, as shown in Figure S7. At 660 nm the observed dynamics fit best to a sum of two exponentials, 230 fs (representing 53% of the decay) and 3 ps (representing 27%), leaving 20% of the amplitude to be accounted for by a long-lived nanosecond offset.

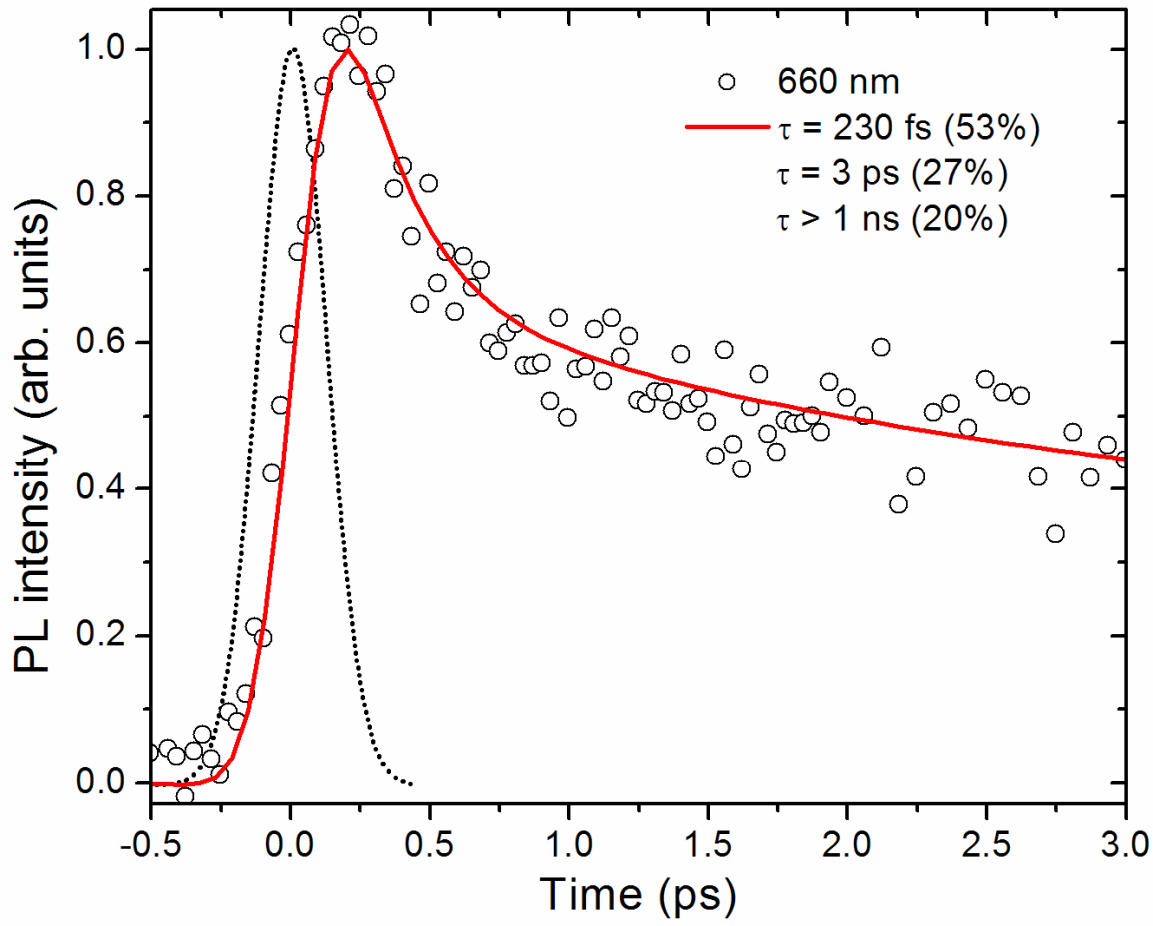

Figure S7: Ultrafast luminescence dynamics at 660 nm on the peak of the steady state PL spectrum for $Ir(dbfliq)_2acac$. Solid line indicates the fit, IRF shown as dotted line. The kinetics fit best to a 230 fs decay component (53%), 3 ps decay (27%) and a nanosecond offset (20%).

7. Ultrafast Transient Absorption Studies

Transient absorption experiments can help support the results found in the ultrafast luminescence work. Detailed evolution of the excited state is less visible in transient absorption dynamics due to the overlap of multiple excited state absorption processes. The most probable observable process is the ^{1}MLCT $\rightarrow$ ^{3}MLCT ISC event, which involves a significant degree of change. Monitoring the transient signal when pumping at 400 nm and probing at 800 nm produces a positive signal (i.e. corresponding to excited state absorption) and the dynamics are shown in Figure S8. The kinetics are fitted by deconvoluting with the IRF (dotted line) and show an exponential decay of 75 fs representing 46% of the total decay, the other 56% being a constant nanosecond offset. The time constant of 75 fs is consistent with the value found for the S_1 luminescence decay, giving good confidence that this is indeed the rate of ISC.

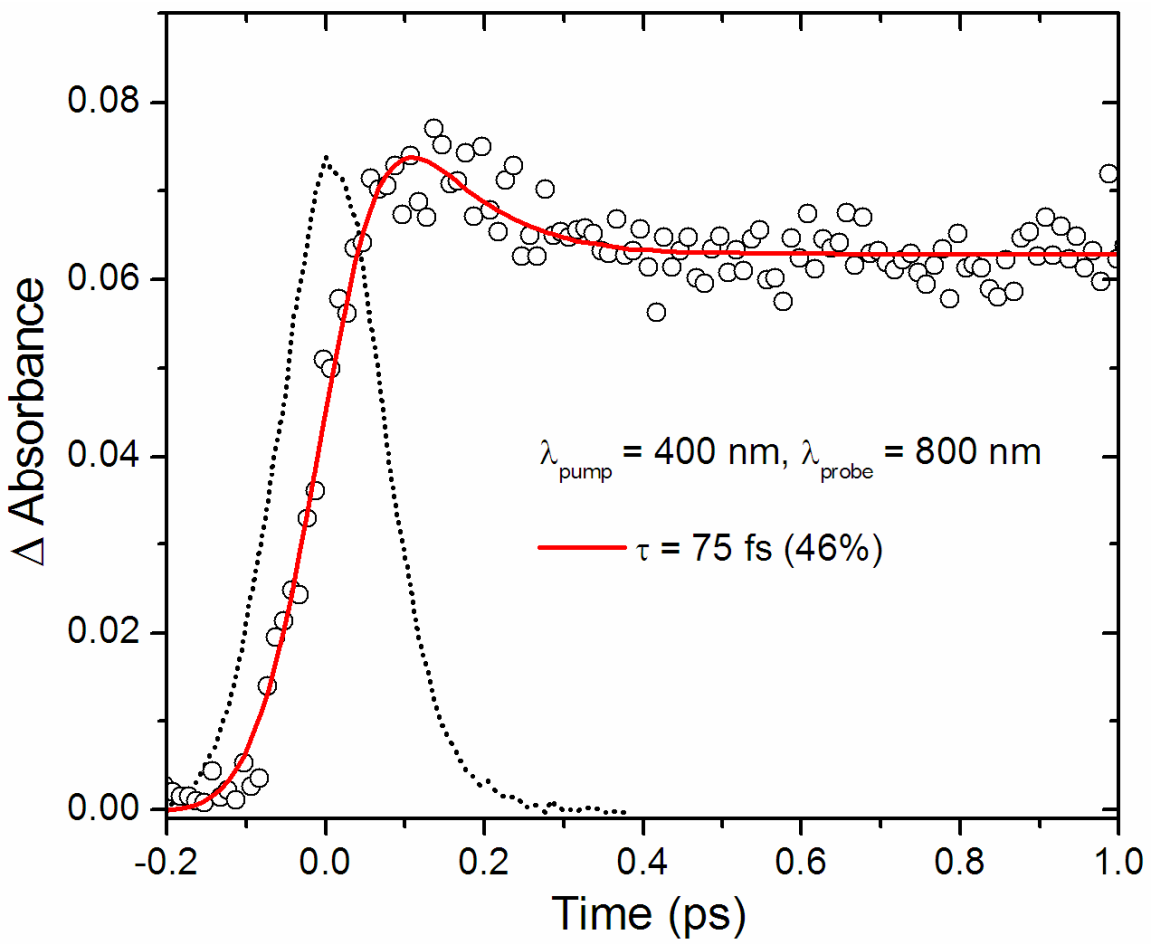

Figure S8: Ultrafast transient absorption kinetics (λ_{pump} = 400 nm, λ_{probe} = 800 nm) for Ir(dbfliq)$_2$acac. Deconvolution of the kinetics with the IRF (dotted line) gives a decay of 75 fs (46% amplitude).

References

(1) Atkins, P. W., *Molecular Quantum Mechanics*. 2 ed.; Oxford University Press: 1983.

(2) Knox, R. S.; van Amerongen, H. *J. Phys. Chem. B* **2002,** *106*, 5289.

(3) Strickler, S. J.; Berg, R. A. *J. Chem. Phys.* **1962,** *37*, 814.

(4) Nozaki, K. *J. Chin. Chem. Soc.-Taip.* **2006,** *53*, 101.

(5) Beechem, J. M.; Gratton, E. *Proc. of SPIE* **1988,** *909*, 77–81.

(6) Lakowicz, J. R., *Principles of Fluorescence Spectroscopy*. 2nd ed.; Kluwer Academic: 1999.

(7) van Stokkum, I. H. M.; Larsen, D. S.; van Grondelle, R. *Biochimica Et Biophysica Acta-Bioenergetics* **2004,** *1657*, 82.

(8) Cannizzo, A.; Blanco-Rodriguez, A. M.; El Nahhas, A.; Sebera, J.; Zalis, S.; Vlcek, J. A.; Chergui, M. *J. Am. Chem. Soc.* **2008,** *130*, 8967.